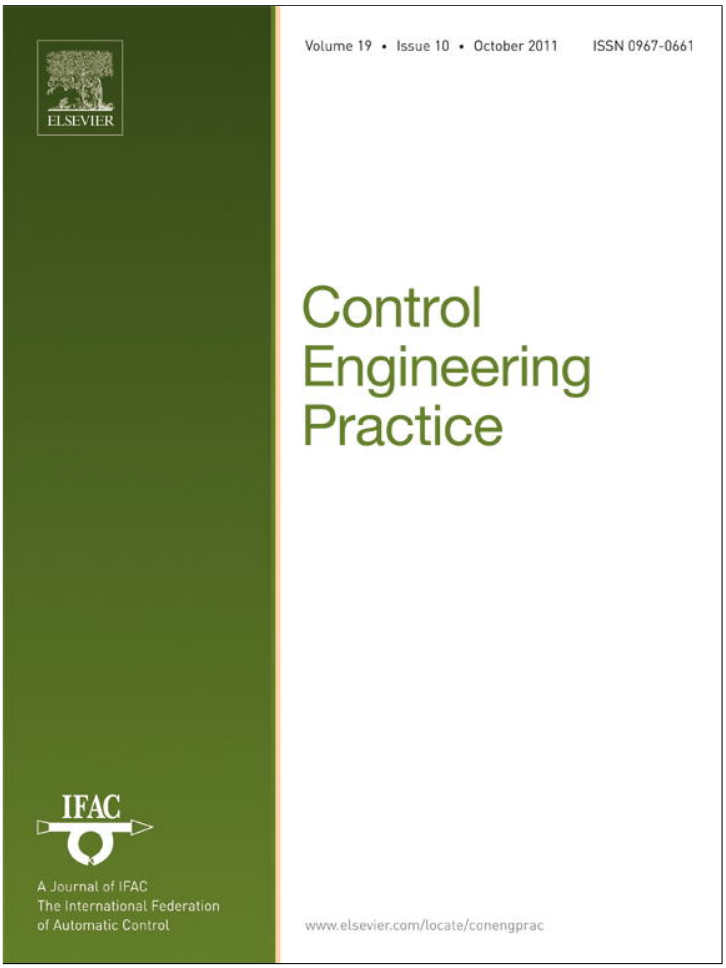

Control Engineering Practice 19 (2011) 1087–1098

Contents lists available at ScienceDirect

Control Engineering Practice

journal homepage: www.elsevier.com/locate/conengprac

Multivariable predictive control for vibrating structures: An application

L. Bossi [a], C. Rottenbacher [b], G. Mimmi [b], L. Magni [a,*]

[a] Dipartimento di Informatica e Sistemistica, Universitá degli Studi di Pavia, via Ferrata 1, 27100 Pavia, Italy
[b] Dipartimento di Meccanica Strutturale, Universitá degli Studi di Pavia, via Ferrata 1, 27100 Pavia, Italy

ARTICLE INFO

Article history:
Received 22 December 2009
Accepted 6 May 2011
Available online 20 July 2011

Keywords:
MPC
LQR
Vibration control
Flexible arm
Multivariable

ABSTRACT

This paper proposes the use of Model Predictive Control (MPC) to control a fast mechanical system. In particular an MPC strategy is applied to a laboratory flexible arm to perform a fast positioning of the end-effector with limited oscillations during the maneuver. The on-line implementation of a fast MPC is obtained with an ad hoc platform based on C++ and MATLAB while the MPC tuning is based on a non-linear model identified and validated with experimental data. The effectiveness of the proposed method is highlighted with some suitable experiments performed on the plant. In particular the comparison with a Linear Quadratic Regulator stresses the advantage of the MPC capability to explicitly handle input and state constraints.This feature guarantees smaller displacements that imply a structure stress reduction.

1. Introduction

Lightweight flexible manipulators have been a widely investigated topic in the field of mechatronic systems. They represent an attractive alternative to heavy and bulky robots in a wide spectrum of applications because of their high payload-to-weight ratio and lower energy consumption. On the other hand, lightweight manipulators are subject to elastic deformations with consequent complex dynamical behaviour. This challenging topic has been deeply investigated and many prototypes of flexible manipulators have been developed in the research centers throughout the world (Lovekin, Hepplerand, & McPhee, 2000; Martins, Mohamed, Tokhi, Sa da Costa, & Botto, 2003; Uchiyama, Konno, Uchiyama, & Kanda, 1990). Although there exists also research finalized to get a technological improvement in industrial or surgical field, majority of the research behind those prototypes is connected to space applications (Book, 1993). The International Space Station has pushed great involvement in this area gathering synergies through the whole world. The Canadarm 2 and the European Robotic Arm are significant examples. Canadarm 2 has a length of 17.6 m, while European Robotic Arm has a length of 11.3 m. Those manipulators work on different parts of the International Space Station. The material used to manufacture the link is the carbon fiber that in an arm of that size gives as result a flexible structure, with consequent oscillations of the arm tip. According to Book definition in Book (1993), a structure is considered flexible when "deflections too large to complete a task persist too long to allow the task to be completed". A way to "solve" this problem is to perform sufficiently slow maneuvers. When the maximum acceptable time for task completion becomes smaller or task content larger, effective control algorithms need to be developed. To reach the current technological level in this area a huge amount of strategies have been developed, handling challenging problems of increasing difficulty that are traditionally classified according to two different criteria. The first classification depends on manipulator structure complexity, defined by the following categories:

- Planar single link flexible manipulators.
- Planar multilink manipulators.
- Multilink manipulators presenting deformations along the three dimensions.

The second classification is based on the aim of the control task to be performed.

- *End-effector regulation problem*. It consists in the achievement of a desired position in an optimal time with respect to the residual vibration at the end of the maneuver.
- *Rest-to-rest motion in a desired fixed time*. In this case, the goal includes also a constraint on the rest-to-rest time.
- *End-effector trajectory tracking*. The end-effector of the arm must follow a desired trajectory in the operative space.

It is proved that a traditional PD with feedback of the motor position stabilizes the system. Nevertheless this strategy is not suitable for the control tasks mentioned above, since oscillations of the end-effector at the end of the maneuver arise. Trying to

* Corresponding author.
E-mail addresses: luca.bossi@unipv.it (L. Bossi), rottenbacher@unipv.it (C. Rottenbacher), giovanni.mimmi@unipv.it (G. Mimmi), lalo.magni@unipv.it (L. Magni).

0967-0661/$ - see front matter © 2011 Elsevier Ltd. All rights reserved.
doi:10.1016/j.conengprac.2011.05.003

solve this problem by using a feedback on the end-effector position, the link results to be actuated at one end and the feedback measure is taken at the other end. Such a system is called *non-colocated* and it is characterized by the presence of a time delay and non-minimum phase (Cannon & Schmitz, 1984). Remarkably, a PD controller cannot stabilize the non-colocated system, due to the presence of real zeros in the positive half-plane in the transfer function from the motor torque to the end-effector position. Trajectory tracking also becomes a difficult task due to non-causal solutions of the inverse dynamic (Bayo, Papadopoulos, Stubbe, & Serna, 1989). Another issue concerns the *infinite dimensionality* of the problem: theoretically the dynamic behavior of a distributed system needs an infinite number of degrees of freedom to be described, even if in real applications a finite model approximation is enough, since high vibration modes own negligible energy content (Meirovitch, 1967). Problems arise when restrictive approximations are adopted, i.e. when high modes neglected in the model are excited during the control task. In this case instability phenomena could appear. This is the so-called *spillover effect* (Balas, 1978). Moreover, *shortcomings* in the construction of a mechanical device could produce important effects on the behavior. An example is the presence of clearance, typically in the joint gear. *Friction* too has important implication on the dynamic behavior of the manipulators. Static or Coulomb friction are the most common, but they are seldom included in the model equations, since viscous or linear friction is easier to model. Anyway some progress has been made in the identification and compensation of Coulomb friction. The majority of used models can describe the manipulator's dynamics in case of small oscillations. Only in recent results new models have been developed trying to describe non-linear dynamics in order to reproduce the system behavior at wider level of velocities and deformations.

To solve the control problem many solutions have been developed during the years such as closed-loop algorithms including Input Shaping feedforward action (Mohamed & Tokhi, 2003), feedback linearization (Wang & Vidyasagar, 1991), strain feedback (Mohamed, Martins, Tokhic, Sá da Costa, & Botto, 2005), passivity based approach (Pereira, Diaz, Cela, & Feliu, 2007), adaptive control (Yuan, Book, & Siciliano, 1989) and regulation schemes based on singular perturbation approach (Bascetta & Rocco, 2006; Siciliano & Book, 1988). Recently, active vibration suppression techniques using smart materials gained most attention and interesting works have been presented (Hassan, Dubay, Li, & Wang, 2007). A remarkable review work on control issues is reported in Benosman and Le Vey (2004) while a panoramic view of developed modeling techniques can be found in Dwivedy and Eberhard (2006). Finally, this paper is focused on the exploration of the effectiveness of multivariable control techniques based on the optimization of a stage cost. They require an accurate model but give the possibility to reach the control objectives just finding suitable values of the weights of the stage cost. In particular Linear Quadratic Regulator (LQR) control and Model Predictive Control (MPC) are considered here. LQR control cannot handle constraints on state or input variables but it can try to satisfy the constraints opportunely modifying the weights. Nevertheless, conservative solutions may occur. The MPC strategy overcomes this limitation, since it can explicitly handle constraints. Traditionally applied to control MIMO systems characterized by slow dynamics, the MPC presents many advantages that could be exploited also by faster systems such as a flexible arm. In fact, since the main limitation of this algorithm is due to its computational burden, strong efforts to set up fast MPC algorithms are increasing (Wang & Boyd, 2008). Moreover, hardware computational capabilities are increasing. For these reasons it is very interesting to test the effectiveness of MPC on fast dynamic systems through experiments performed on laboratory plants. Since MPC can handle constraints, optimal performance can be reached also in the presence of actuator saturations and bounds on the maximum oscillation during the maneuver can be specified in explicit form. This feature guarantees smaller displacements that imply a structure stress reduction. Hence, the flexible manipulator can be considered a good platform to test the effectiveness of the MPC technique. To the best of our knowledge the literature in this field is focused on simulation results (Boscariol, Gasparetto, Zanotto, 2010). Only an experimental result concerning the active vibration suppression approach has been obtained in Hassan et al. (2007).

Model based approach for flexible manipulators control is affected by the following intrinsic limitations:

- the complexity of the control algorithm increases significantly with the system order;
- the stability of the closed-loop system is sensitive to model parameter uncertainties, to changes in the robot payload, to high-order unmodeled dynamics as the control bandwidth is raised (spillover effects).

Nevertheless, it is well known that MPC strategies own inherent robustness properties, so that the main dynamics of a system can be approximated with enough accuracy with low-order models. Hence, the aim of this paper is to highlight the effectiveness of multivariable approaches, through the achievement of the following goals:

- to build an accurate simulator of a single link flexible apparatus validated on experimental data, necessary for the application of a model based control algorithm;
- to compare in simulation LQR and MPC control schemes to show the performance improvement introduced by handling constraints;
- to test the effectiveness of the MPC scheme on the experimental plant.

Concerning the second goal, it is worth to remark that the comparison of two different control techniques is a critical issue, since one can be better tuned than the other. Nevertheless, using the LQR with the same cost function and the same sample time of the MPC, it is possible to show in a fair way the advantages of explicit consideration of the constraints, avoiding the problem of different tunings.

The single link planar manipulator considered in this paper is a part of the plant designed in the context of an ASI (Italian Space Agency) multi-objective research contract (Bernelli-Zazzera et al., 2001). The goal of the overall research was the design and the realization of an experimental device for the validation of control techniques applied to flexible articulated systems. The robotic arm is suspended on a suitable air-pad, floating on a glass planar surface to reduce friction effects. This designed plant works in the same conditions of a system operating in a microgravity environment, in which the experimental tests shall be carried out. In fact, the presence of the air-pad counteracts the effect of the gravity field, supporting the whole weight of the arm, without any friction with the table.

The paper is organized as follows: Section 2 gives a detailed description of the experimental apparatus. A linear mathematical model, derived by means of the assumed mode methods and complemented with a non-linear friction model is presented in Section 3. Then, in Section 4, the parameters identification procedure is described and carried out. In particular suitable experiments are designed in order to identify the parameters of the model that cannot be measured or analytically computed. The identified model is then validated: this step is reported in Section 5. The adopted MPC formulation is described in Section 6. Experimental control results are reported in Section 7. Finally, conclusions are presented.

2. Experimental apparatus

The experimental device used for the experimental tests (Fig. 1) is a part of the TEMSRAD (Testbed for Microgravity Simulation in Robotic Arm Dynamics) (Mimmi, Rottenbacher, & Bonandrini, 2008). It consists of a flexible robotic arm driven by a brushless servomotor, operating in a working space compatible with the volume of a standard Express Pallet Adapter (EPA) designed for on board experiments on the International Space Station (ISS).

The robotic arm is suspended on a special air-pad floating on a planar friction-free glass surface in order to simulate the dynamic behavior in a microgravity environment. In this way the torsional vibration components are reduced even with a payload mounted at the end point of the manipulator. The links in kevlar fiber tissue are very flexible in the operating plane; on the contrary, they can be considered rigid in the other directions. The robotic arm is actuated with a Kollmorgen 713-RBH brushless motor with a maximum torque of 0.3 Nm, driven by a sinusoidal digital servoamplifier Danhaer Motion Servostar S606, capable to produce a maximum current of 6 A. An internal current loop, realized by the servo amplifier, with parameters tuned by the manufacturer, provides the control torque of the motor. A resolver is mounted on motor axis to furnish the rotor position, needed by the amplifier in order to produce the right signal for motor driving. The system is equipped with strain gauges in a full-bridge configuration mounted both at the base and in the middle of the link, to measure deflections and with a potentiometer mounted on motor axis, to measure the angular position of motor shaft. The developed application for the on-line implementation of the MPC algorithm is a C++ application interfaced with MATLAB through the MATLAB Engine libraries.

3. Model description

3.1. Linear model equations

Using the reference system X_p, Y_p (see Fig. 2) passing through the center of mass for the energy terms computations, the following boundary value problem is obtained applying the Hamilton Principle (Meirovitch, 1967):

$$\begin{cases} EIw_p''''(x,t)+\rho(\ddot{w}_p(x,t)+x\ddot{\alpha}(t))=0 \\ \tau(t)-J\ddot{\alpha}(t)=0 \end{cases} \quad (1)$$

where x and t are, respectively, spatial and time coordinate, $w_p(x,t)$ is the link deflection, ρ is the linear mass density, $\tau(t)$ is the applied torque, $\alpha(t)$ is the angle of the center of mass, E is the Young modulus, I is the cross section inertia and J is the total inertia of the system that includes the inertia moment of the joint, the inertia of the air-pad support mounted at the end of the beam that connects the kevlar link to the air-pad and the inertia of the beam. Assuming a separated variable solution, for the expansion theorem, the solution of (1) can be represented by an absolutely and uniformly convergent series in the eigenfunctions in the form

$$w_p(x,t)=\sum_{i=1}^{\infty}\phi_{pi}(x)\delta_{pi}(t)$$

where $\phi_{pi}(x)$ is the exact eigenfunction obtained solving the eigenvalue problem associated to (1) and $\delta_{pi}(t)$ is the time dependent term. Truncating the series at n terms the following system can be derived (Canudas de Wit, Bastin, & Siciliano, 1996):

$$\begin{cases} J\ddot{\alpha}(t)=\tau(t) \\ \ddot{\delta}_{pi}(t)+2\xi\omega_i\dot{\delta}_{pi}(t)+\omega_i^2\delta_{pi}(t)=\phi'_{pi}(0)\tau(t) \end{cases}$$

$i=1,\ldots,n$ where ω_i^2 are the eigenvalues of the system which correspond to the squares of angular frequencies and n is the number of the considered modes of vibration. Note that the damping ratio ξ includes the dissipation effects due to the internal frictions of the link, the friction between the air-pad and the table and the air resistance. However, it does not represent the damping of the overall structure, in fact, the effect of other friction sources such as the friction of the motor will be described separately in the next subsection. As it will be clarified in the model identification section, the decision to consider some friction phenomena in the damping ratio ξ and some other explicitly in the friction model is driven by the possibility to design experiments apt to identify them.

In order to obtain the system description with respect to the reference system X_cY_c (see Fig. 2) the following change of coordinates can be done:

$$\phi_{ci}(x)=\phi_{pi}(x)-x\phi'_{pi}(0)$$

$$\delta_{ci}(t)=\delta_{pi}(t)=\delta_i(t)$$

where $\phi_{ci}(x)$ is the exact eigenfunction and $\delta_{ci}(t)$ is the time dependent term in the new reference system.

In this way the hub angle $\theta_{hub}(t)$, the tip angle $\theta_{tip}(t)$ and the deflection at the end point of the end-effector in the clamped reference system $w_c(l,t)$ can be derived as follows:

$$\begin{cases} \theta_{hub}(t)=\alpha(t)+\sum_{i=1}^{n}\phi'_{pi}(0)\delta_i(t) \\ w_c(l,t)=\sum_{i=1}^{n}\phi_{ci}(l)\delta_i(t) \\ \theta_{tip}(t)=\theta_{hub}(t)+\dfrac{w_c(l,t)}{l}=\alpha(t)+\dfrac{w_p(l,t)}{l} \end{cases}$$

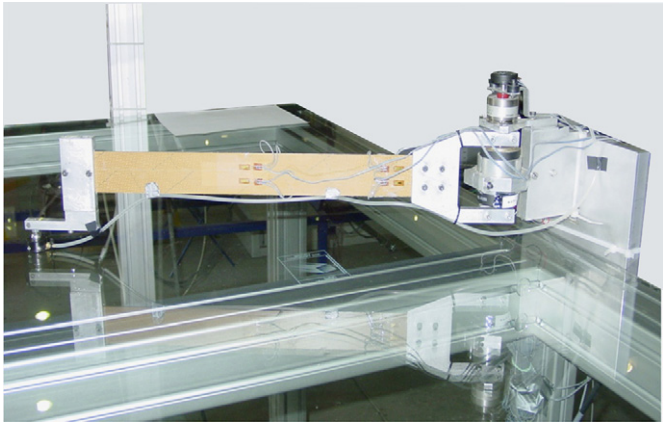

Fig. 1. Experimental test bed.

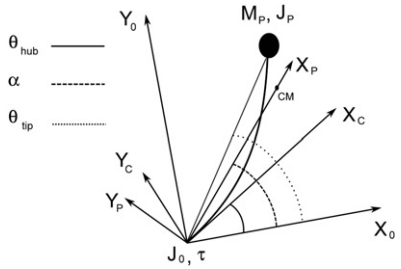

Fig. 2. Single link manipulator.

where

$$w_p(l,t) = \sum_{i=1}^{n} \phi_{pi}(l)\delta_i(t)$$

Finally, defining the state and the output vectors

$$\chi = [\alpha \ \ \delta_1 \ \ \ldots \ \ \delta_n \ \ \dot{\alpha} \ \ \dot{\delta}_1 \ \ \ldots \ \ \dot{\delta}_n]'$$

$$y = [\theta_{hub} \ \ w_c(l,\cdot)]'$$

the system equations can be rewritten in the following state-space representation:

$$\begin{cases} \dot{\chi}(t) = A\chi(t) + B\tau(t) \\ Y(t) = C\chi(t) \end{cases} \tag{2}$$

where

$$A = \begin{bmatrix} 0 & 0 & \ldots & 0 & 1 & 0 & \ldots & 0 \\ 0 & 0 & \ldots & 0 & \vdots & 1 & \ldots & 0 \\ \vdots & \vdots & \ddots & \vdots & \vdots & \vdots & \ddots & \vdots \\ 0 & 0 & \ldots & 0 & 0 & 0 & \ldots & 1 \\ 0 & 0 & \ldots & 0 & 0 & 0 & \ldots & 0 \\ 0 & -\omega_1^2 & \ldots & 0 & 0 & -2\xi_1\omega_1 & \ldots & 0 \\ \vdots & \vdots & \ddots & \vdots & \vdots & \vdots & \ddots & \vdots \\ 0 & 0 & \ldots & -\omega_n^2 & 0 & 0 & \ldots & -2\xi_n\omega_n \end{bmatrix}$$

$$B = \begin{bmatrix} 0 & 0 & \ldots & 0 & \frac{1}{J} & \phi'_{p1}(0) & \ldots & \phi'_{pn}(0) \end{bmatrix}$$

$$C = \begin{bmatrix} 1 & \phi'_{p1}(0) & \ldots & \phi'_{pn}(0) & 0 & 0 & \ldots & 0 \\ 0 & \phi_{c1}(l) & \ldots & \phi_{cn}(l) & 0 & 0 & \ldots & 0 \end{bmatrix}$$

3.2. Friction model

The friction effect has been described with the classical Karnopp model (Olsson, Aström, Canudas-de Wit, Gäfvert, & Lischinsky, 1998), which is sufficiently accurate but also simple enough to be identified from real data.

Karnopp friction model is defined by the following system of equations:

$$\tau_f f = \begin{cases} \tau_c \mathrm{sgn}(\dot{\theta}_{hub}) & \text{if } |\dot{\theta}_{hub}| > d \\ \tau_e & \text{if } |\tau_e| < \tau_s, \quad |\dot{\theta}_{hub}| < d \\ \tau_s \mathrm{sgn}(\dot{\theta}_{hub}) & \text{otherwise} \end{cases} \tag{3}$$

where τ_e is the external force applied to the system, τ_f is the overall friction torque, τ_s the static friction, τ_c the Coulomb friction, while the range $[-d,d]$ defines the velocity deadzone.

Then, a compact form of the friction model is introduced that is easier to be graphically represented as in Fig. 3.

$$\tau_f = \begin{cases} \tau_c \mathrm{sgn}(\dot{\theta}_{hub}) & \text{if } |\dot{\theta}_{hub}| > d \\ \mathrm{sat}(\tau_e)\mathrm{sgn}(\dot{\theta}_{hub}) & \text{otherwise} \end{cases}$$

where

$$\mathrm{sat}(\tau_e) = \begin{cases} |\tau_e| & \text{if } |\tau_e| < \tau_s \\ \tau_s & \text{otherwise} \end{cases}$$

3.3. Actuator limitation

Another non-linear effect is due to the saturation on the control variable (i.e. $\tau_{min} \le \tau(t) \le \tau_{max}$) due to the limit on the torque available by the motor.

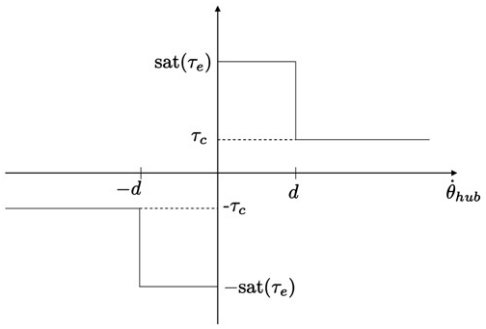

Fig. 3. Friction model.

4. Model identification

In this section the values of the parameters of the plant reported in Table 2 are derived. In particular the mass of the payload m_p, the linear mass density of the beam ρ, the beam length l, the cross area inertia I are easily measurable from the plant; the mass moment of inertia of the payload J_p and the hub inertia J_0 are computed starting from the geometrical and physical characteristics of the system, while the Young modulus E, the damping ratio ξ and the friction are identified on the base of experimental data obtained with suitable experiments performed both on single parts of the plant and on the whole plant.

4.1. Young modulus characterization

The identification of the Young modulus E requires a beam test. In fact the theoretical estimation of this parameter may be quite different from the real one because the composite material link has peculiar characteristics strongly dependent on the manufacturing process. The composite materials are also subject to aging that produces link stiffness loss. The beam test is performed as follows: the link is clamped at one end and increasing mass payloads are hanged up at the free end of the link. Starting from the relationship between the applied force F and the displacement Δ we can find the Young modulus by the following equation derived by structural mechanics (Gurtin, 1981)

$$E = \frac{Fl^3}{3I\Delta}$$

where $F=mg$ is the force acting on the end point of the beam; m and g are, respectively, the total applied mass and the gravity acceleration, with $m = m_1 + m_2$ where m_1 is the weight of the applied mass reported in Table 1, while $m_2 = 0.019$ kg is the weight of a thin plate, inserted in the cavity of the link, in correspondence of the air-pad support to avoid beam damages in that point. The obtained values of E summarized in Table 1 highlight a quite linear model of the elasticity of the beam, at least in the range of displacements where the tests have been performed. This characteristic satisfies the linearity assumptions introduced in the previous section. Nevertheless other experiments made on the overall system show the presence of a non-linear behavior that can be observed extending the upper and the lower bound of the deflections range. In particular different chirp signals with increasing amplitude are applied to the motor as torque references. As can be seen in Fig. 4 the wider the produced displacement, the lower is the frequency at which the resonance phenomenon occurs. In conclusion the most suitable choice seems to be $E = 6.408$ GPa.

Table 1
Young modulus characterization.

Applied mass (kg)	Displacement (m)	Young modulus E (GPa)
0.005	0.023	6.6867
0.010	0.029	6.4081
0.015	0.034	6.4081
0.020	0.039	6.4081
0.025	0.044	6.4081

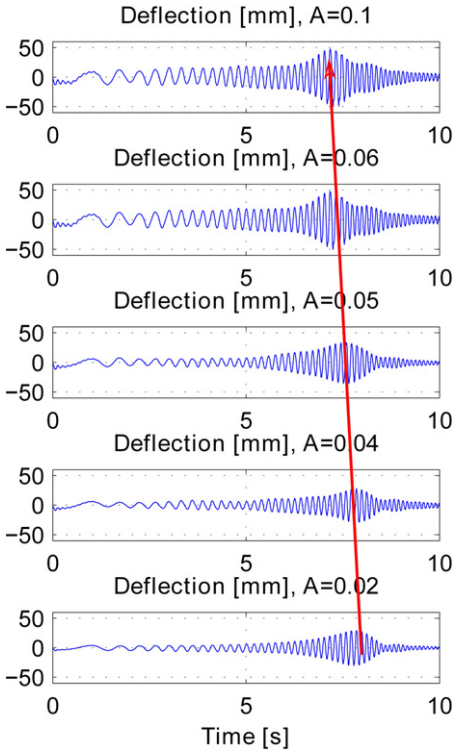

Fig. 4. Resonance frequency shift.

4.2. Relevant modes identification

Through the knowledge of the parameters identified so far it is possible to compute the natural frequencies of the system. In particular it is obtained $\omega_1 = 45.65$ rad/s, $\omega_2 = 114.47$ rad/s and $\omega_3 = 266.47$ rad/s corresponding to $f_1 = 7.26$ Hz the first one, $f_2 = 18.21$ Hz the second one and $f_3 = 42.41$ Hz the last one. Anyway it is important to look for experimental evidences to check the reliability of these theoretical values and to understand which modes of vibration are actually excited, within a desired range of frequencies. To this aim, the *Matlab System Identification Toolbox* is used to perform the spectral analysis of plant data obtained through suitable experiments. In particular a chirp signal is applied as motor torque reference. The frequency of the signal increases linearly with the time, passing from 1 to 50 Hz in 30 s. The test is repeated two times, first with the air-pad and then removing the air-pad. In these tests link deformation is measured using the strain gauges mounted in the middle of the link and the other ones mounted close to the motor. In this way four signals are obtained and analyzed through spectral analysis. The signal spectra are plotted in Fig. 5 using different line styles according to the legend. Looking at the figure, it is possible to recognize the first mode of vibration, in correspondence to the same frequency resulting from the analytical computation, while another relevant component appears at about 30 Hz, detected by the "Base" strain-gauge, that is very different from the second analytical frequency. To better understand this phenomenon a second experiment is performed removing the air-pad at the end of the arm to excite potential torsional vibration modes. From the spectral analysis reported in Fig. 5 it is possible to observe that the presence of the air-pad reduces the entity of the peak at 30 Hz. This experiment highlights that the observed peak is due to a torsional mode that is not described by the model that takes into account only flexural vibrations. It is also possible to see that the "Base" strain-gauge detects a peak between 16 and 18 Hz, very close to f_2, even if with a negligible energy content. These tests and the spectral analysis show the relevance of the torsional mode of vibration without air-pads, that limits closed-loop performance. Hence, the robotic arm is equipped with air-pads. Moreover, with this configuration the first flexural mode of vibration is enough to obtain a reliable model. Since only one vibration mode is assumed, the measure of the displacement of the tip is obtained through an empirical relation with the link deformation measurement provided by the strain gauges close to the motor.

4.3. Damping identification

As it is stated in the previous section the damping ratio ξ describes also the effect of some friction terms. The ones due to the motor rotation are not involved in it. Then in order to identify ξ, the joint has been clamped and given an initial displacement to the end-effector, the resulting free vibrations are analyzed. Applying the logarithmic decay method (Rao, 2003) the damping ratio is identified with value $\xi = 0.034$.

4.4. Friction identification

To obtain the friction model of the plant, described in (3), three parameters should be identified: the static friction coefficient τ_s,

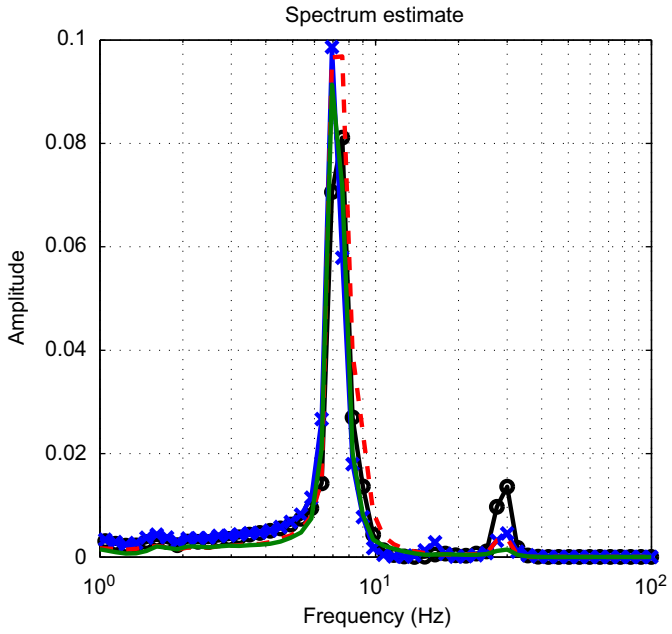

Fig. 5. Frequency response of the manipulator structure obtained applying a chirp signal in the range [0, 50] [Hz]. Red line: response obtained from the strain gauges placed in the middle of the link during the test without air-pad. Green line: response obtained from the strain gauges placed in the middle of the link during the test with air-pad. Blue line: response obtained from the strain gauges placed close to the base of the link during the test with air-pad. Black line: response obtained from the strain gauges placed close to the base of the link during the test without air-pad. (For interpretation of the references to color in this figure legend, the reader is referred to the web version of this article.)

the velocity threshold d and Coulomb friction coefficient τ_c. The first parameter is identified applying increasing torque until the joint motion begins. The torque value that is necessary to move the motor will be the value assigned to τ_s. The value d is usually very small and difficult to estimate. We have arbitrarily chosen it equal to $0.001\,^\circ/\mathrm{s}$. The procedure to identify τ_c follows the sequent steps. First an initial displacement is given to the tip of the manipulator with the joint free to rotate and the resulting vibrations are analyzed through the method of the logarithmic decay. In this way an equivalent damping ratio ς of the whole plant is identified. It includes the vibration damping effect due to the motor friction. Then several simulations for different increasing values of τ_c are performed. Finally, the value of τ_c that better reproduces in simulation the equivalent damping of the real plant is chosen.

5. Model validation for control

Once every parameters of the model are identified, it is necessary to validate the whole model, required by the synthesis of feedback control laws. It is well known that in this respect it is important to have a good model in the range of frequencies close to the closed-loop bandwidth while it is not necessary to have a very precise model at low or high frequencies. For this reason a closed-loop validation is performed using a multi variable controller based on an LQR control law complemented with a Kalman observer.

5.1. Discrete LQR formulation

Let be considered the discretized version of the system (2) including only one vibration mode, as result from the identification procedure.

$$\begin{cases} x(k+1) = Ax(k) + Bu(k), & k \geq \overline{k} \\ y(k) = Cx(k) \end{cases} \tag{4}$$

with $x \in \mathbb{R}^4$, $u \in \mathbb{R}$, $y \in \mathbb{R}^2$ and A, B, C matrices with suitable dimensions obtained through ZOH discretization with sampling time $T_s = 0.03$ s. The LQR control problem consists in finding at each sampling instant k the control $u(k)$ solving the following optimization problem:

$$\underset{u(\cdot)}{\operatorname{argmin}} J(x(\overline{k}), u(\cdot)) \tag{5}$$

with

$$J(x(\overline{k}), u(\cdot)) = \sum_{k=\overline{k}}^{\infty} x(k)'Qx(k) + u(k)'Ru(k)$$

where $Q = Q' \geq 0$, $R = R' > 0$ are the weighting matrices having suitable dimensions, to be chosen as design parameters, and $u(\cdot)$ is the control sequence on infinite horizon. The resulting feedback law, solution of (5), is

$$u^o(\overline{k}) = -\overline{K}x(\overline{k}) \tag{6}$$

where

$$\overline{K} = (R + B'\overline{P}B)^{-1}B'\overline{P}A \tag{7}$$

and $\overline{P}$ is the solution of the steady Riccati equation.

$$\overline{P} = A'\overline{P}A + Q - A'\overline{P}B(R + B'\overline{P}B)^{-1}\overline{B}\overline{P}A \tag{8}$$

Moreover, since the state of the system is not completely accessible, a Kalman estimator is designed.

5.2. Kalman estimator

Defining $\tilde{x}(k+1|k)$ the estimation of the state depending on the knowledge of input and output at the instant k, it is possible to derive the following equation of the discrete time Kalman estimator:

$$\tilde{x}(k+1|k) = A\tilde{x}(k|k-1) + Bu(k) + L[y(k) - C\tilde{x}(k|k-1)]$$

where, given the covariance of the noises on the state and output equations, the gain L is derived by solving a standard Riccati equation. It is important to notice that the covariance of the noise measure can be obtained by the characteristic of the sensor, while there is no way to have an estimation of the noise of the state equation. Hence, the choice of the covariance is a tuning parameter that must be chosen in order to modify the gain of the observer. This has been done with a trial and error procedure first on the simulator and then on the real plant.

5.3. Validation tests

The first validation test consists in a motor rotation maneuver of 120°. Comparisons between simulated and experimental responses are shown in Figs. 6,7,8. Looking at Fig. 6, it is possible to observe that the behavior of $\theta_{hub}(t)$ described by the model reproduces the real behavior of the plant, using the same input torque (see Fig. 7). An important difference in the deflection amplitude between the simulated and the real response is highlighted in Fig. 8. Nevertheless the model predicts with high accuracy the vibration frequency and the oscillations decay time. Two further validation tests are designed on the base of the following observation. The motor hub response reported in Fig. 6 is characterized by a settling time of about 2 s, and by a response similar to the one of a second-order linear system. On the base of this information, the characteristic frequency ω_c of the closed-loop plant is estimated equal to 0.35 Hz. Then, suitable reference signals are applied in order to better validate the plant in proximity of the closed-loop characteristic frequency. Two sinusoids at 0.2 and 0.4 Hz with mean value 90° are used. The resulting comparisons between the simulated and the real plant responses are in Figs. 9–14.

In particular, Figs. 11 and 14 confirm the deflection overestimation results, previously highlighted (see Fig. 8). Moreover

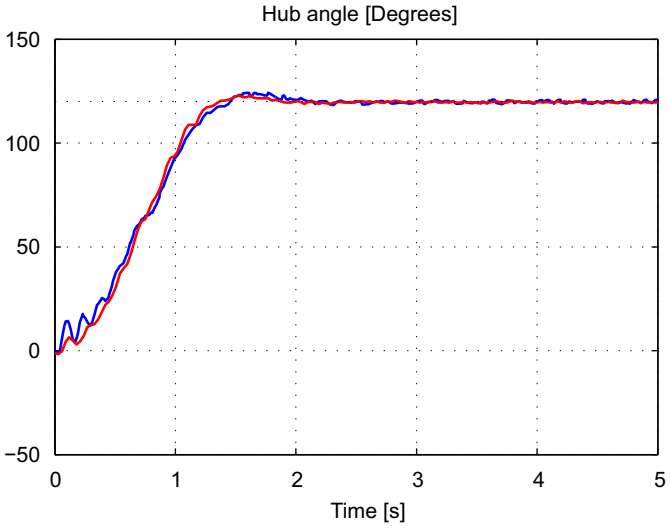

Fig. 6. Validation test with LQR: 120° step response. Blue line: simulation. Red line: experimental result. (For interpretation of the references to color in this figure legend, the reader is referred to the web version of this article.)

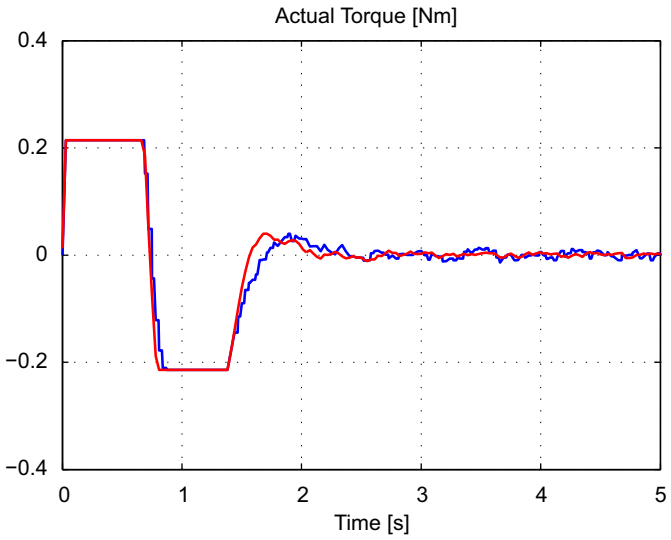

Fig. 7. Validation test with LQR: 120° step response. Blue line: simulation. Red line: experimental result. (For interpretation of the references to color in this figure legend, the reader is referred to the web version of this article.)

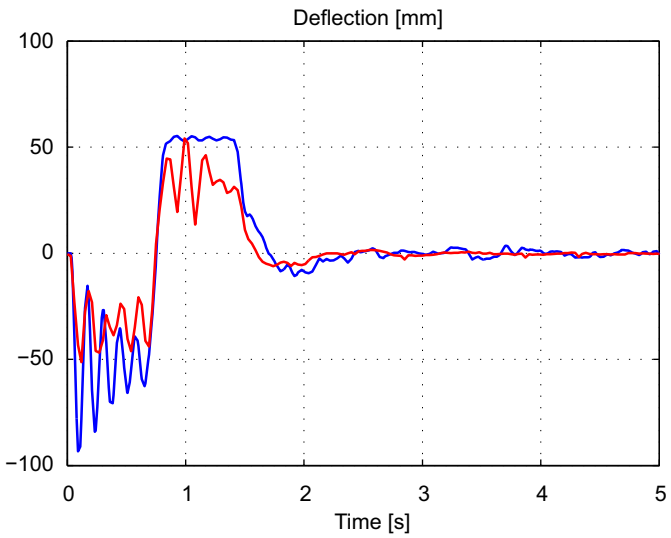

Fig. 8. Validation test with LQR: 120° step response. Blue line: simulation. Red line: experimental result. (For interpretation of the references to color in this figure legend, the reader is referred to the web version of this article.)

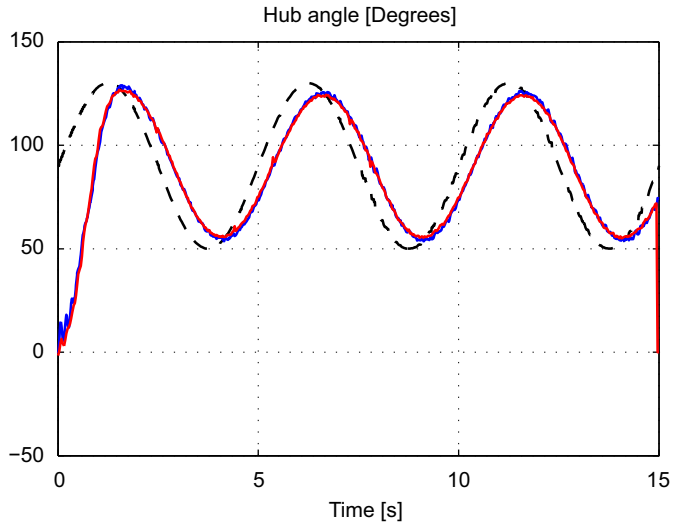

Fig. 9. Validation test with LQR: 0.2 Hz sinusoidal response. Blue line: simulation. Red line: experimental result. (For interpretation of the references to color in this figure legend, the reader is referred to the web version of this article.)

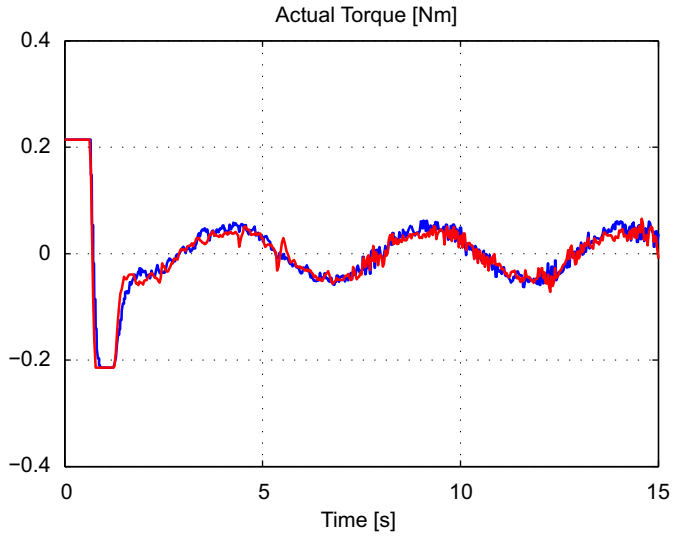

Fig. 10. Validation test with LQR: 0.2 Hz sinusoidal response. Blue line: simulation. Red line: experimental result. (For interpretation of the references to color in this figure legend, the reader is referred to the web version of this article.)

doing a comparison between Figs. 9 and 12, it is possible to observe that a better accuracy is obtained for the 0.2 Hz excitation of the system. However, the model catches with enough accuracy the main dynamics of the real system for the 0.4 Hz higher frequency excitation signal as well (see Fig. 14).

6. Model predictive control

In this section the MPC is proposed to control the plant. The MPC formulation is presented first. Then, an ad hoc platform for the online implementation of the MPC is designed and the obtained experimental results are shown and discussed.

Let be considered the dynamic system described by Eqs. (4), the state and control constraints,

$$|x(k)| < x_{bnd}, \quad k > \overline{k}$$

$$|u(k)| < u_{bnd}, \quad k > \overline{k}$$

where x_{bnd} and u_{bnd} are vectors in $\mathbb{R}^4$ and $\mathbb{R}$, respectively. The operator $|\cdot|$ works component wise. Moreover, letting $U(\overline{k}) = \{u(\overline{k}), u(\overline{k}+1), \ldots, u(\overline{k}+N-1)\}$, the stage cost for the MPC is

$$J(x(\overline{k}), U(\overline{k})) = \sum_{k=\overline{k}}^{\overline{k}+N-1} (\|x(k)\|_Q^2 + \|u(k)\|_R^2) + \|x(k+N)\|_S^2 \tag{9}$$

where $Q = Q' \geq 0$, $R = R' > 0$, $S = S' \geq 0$ are suitable dimensions matrices. The expression $\|x\|_Q^2$ is the short representation of the quadratic form x^{TQx}. The positive integer N is usually defined *prediction horizon*. The control problem solution at each sampling time $\overline{k}$ consists in the determination of the optimal control sequence $U^o(\overline{k}) = \{u^o(\overline{k}), u^o(\overline{k}+1), \ldots, u^o(\overline{k}+N-1)\}$ obtained solving the constrained optimization problem

$$\min_{U(\overline{k})} J(x(\overline{k}), U(\overline{k})) \tag{10}$$

subject to (4),

$$|x(k)| < x_{bnd}, \quad k \in [\overline{k}, \overline{k}+N] \tag{11}$$

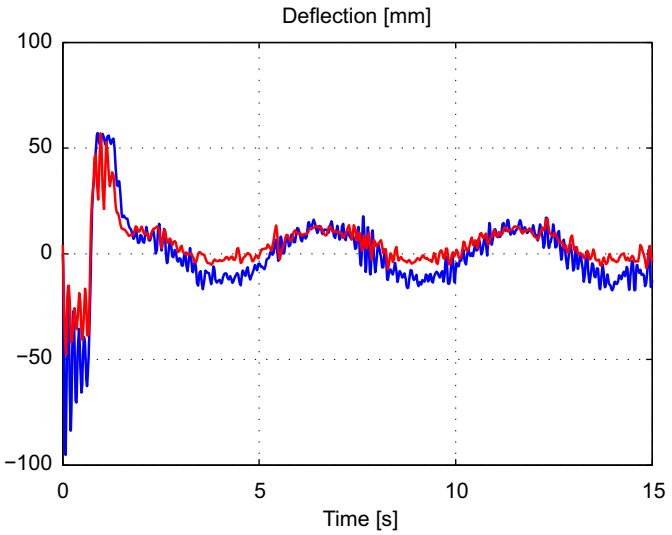

Fig. 11. Validation test with LQR: 0.2 Hz sinusoidal response. Blue line: simulation. Red line: experimental result. (For interpretation of the references to color in this figure legend, the reader is referred to the web version of this article.)

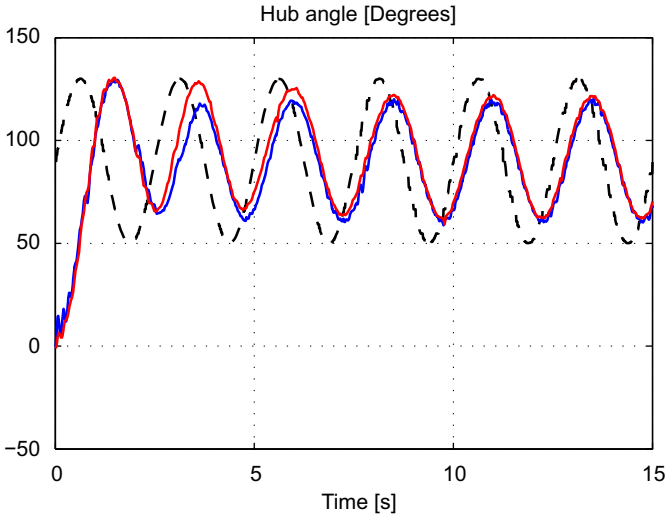

Fig. 12. Validation test with LQR: 0.4 Hz sinusoidal response. Blue line: simulation. Red line: experimental result. (For interpretation of the references to color in this figure legend, the reader is referred to the web version of this article.)

$$|u(k)| < u_{bnd}, \quad k \in [\overline{k}, \overline{k}+N-1] \tag{12}$$

Finally the MPC control law is obtained applying the *Receding Horizon* (*RH*) strategy which works as follows: at the instant $\overline{k}$ the optimal sequence $U^o(\overline{k})$ on the finite horizon $[\overline{k}, \overline{k}+N]$ is computed, but only its first element is applied as input to the system. At the next instant $\overline{k}+1$ the solution is recomputed over the prediction horizon $[\overline{k}+1, \overline{k}+N+1]$ and so on for every instants k during the runtime. Through the *RH* approach a time-invariant state feedback control law is obtained.

6.1. Equivalence between unconstrained MPC and LQR

A possible solution of the unconstrained problem (10) can be obtained through the application of the Riccati equation. It is given by

$$u^o(\overline{k}) = -K(0)x(\overline{k}) \tag{13}$$

where

$$K(0) = (R+B'P(1)B)^{-1}B'P(1)A$$

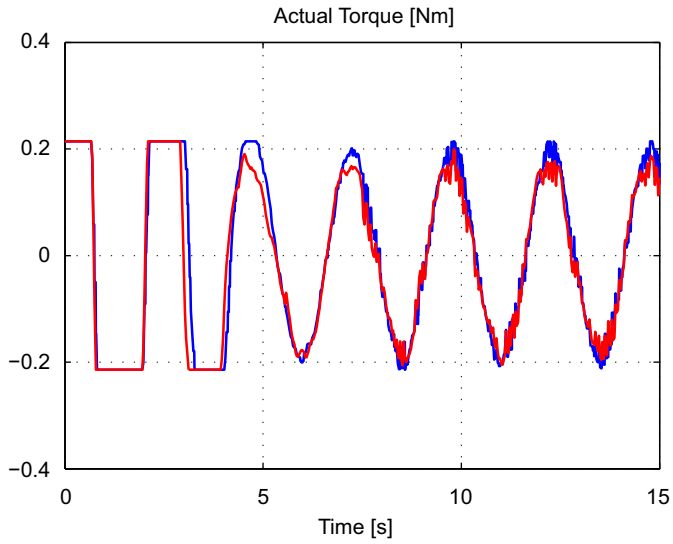

Fig. 13. Validation test with LQR: 0.4 Hz sinusoidal response. Blue line: simulation. Red line: experimental result. (For interpretation of the references to color in this figure legend, the reader is referred to the web version of this article.)

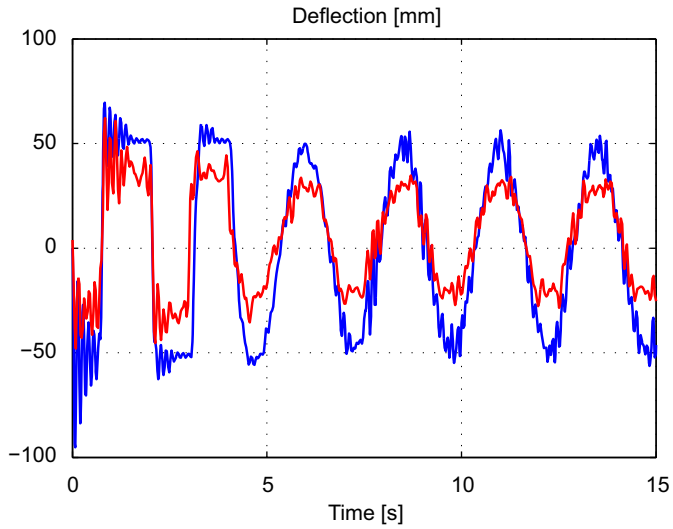

Fig. 14. Validation test with LQR: 0.4 Hz sinusoidal response. Blue line: simulation. Red line: experimental result. (For interpretation of the references to color in this figure legend, the reader is referred to the web version of this article.)

with

$$P(i) = Q + A'P(i+1)A - A'P(i+1)B(R+B'P(i+1)B)^{-1}B'P(i+1)A \tag{14}$$

where $P(N) = S$ is the final weight. Choosing the final weight S of (14) equal to $\overline{P}$, solution of the steady-state Riccati equation (8), it is easy to see the identity $P(1) = \overline{P}$ so that the MPC control law results the same of the LQR one. This proves that with a suitable choice of the final weight S, the MPC reaches the same performance of the LQR synthesized using the same weighting matrices Q and R. The main improvement obtained with the MPC is expected when constraints are explicitly handled. In this case the MPC is supposed to be able to reach and improve the LQR performance with respect to a desired criterion, without modifying the algorithm tuning. In the next section the full constrained MPC problem (10), (11), (12) is solved.

6.2. Constrained MPC

If constraints are considered the solution of the optimization problem cannot be obtained through the solution of the Riccati

equation and it is necessary to consider an *open-loop* solution that allows to take explicitly into account constraints on both input and state variables. Let be considered the model (4). The state evolution of the system, according to the Lagrangian equation, is given by

$$x(k) = A^{(k-\bar{k})}x(\bar{k}) + \sum_{i=\bar{k}}^{k-1} A^{k-i-1}Bu(i) \tag{15}$$

and defining

$$\mathcal{A} = \begin{bmatrix} A \\ A^2 \\ \vdots \\ A^{N-1} \\ A^N \end{bmatrix}$$

$$\mathcal{B} = \begin{bmatrix} B & 0 & 0 & \dots & 0 & 0 \\ AB & B & 0 & \dots & 0 & 0 \\ \vdots & \vdots & \vdots & \dots & \vdots & \vdots \\ A^{N-2}B & A^{N-3}B & A^{N-4}B & \dots & B & 0 \\ A^{N-1}B & A^{N-2}B & A^{N-3}B & \dots & AB & B \end{bmatrix}$$

$$X(\bar{k}) = \begin{bmatrix} x(\bar{k}+1) \\ x(\bar{k}+2) \\ \vdots \\ x(\bar{k}+N-1) \\ x(\bar{k}+N) \end{bmatrix}$$

the expression (15) can be written in matricial form as

$$X(\bar{k}) = \mathcal{A}x(\bar{k}) + \mathcal{B}U(\bar{k}) \tag{16}$$

The optimization problem to solve is

$$\min_{U(\bar{k})} J(x(\bar{k}),U(\bar{k})) = \min_{U(\bar{k})} \bar{J}(x(\bar{k}),U(\bar{k})) \tag{17}$$

where $\bar{J}(x(\bar{k}),U(\bar{k}))$ is the cost function (9) written in the compact way

$$\bar{J}(x(\bar{k}),U(\bar{k})) = X'(\bar{k})\mathcal{Q}X(\bar{k}) + U'(\bar{k})\mathcal{R}U(\bar{k}) \tag{18}$$

with

$$\mathcal{Q} = \begin{bmatrix} Q & 0 & \dots & 0 & 0 \\ 0 & Q & \dots & 0 & 0 \\ \vdots & \vdots & \ddots & \vdots & \vdots \\ 0 & \dots & 0 & Q & 0 \\ 0 & \dots & 0 & 0 & S \end{bmatrix}$$

$$\mathcal{R} = \begin{bmatrix} R & 0 & \dots & 0 & 0 \\ 0 & R & \dots & 0 & 0 \\ \vdots & \vdots & \ddots & \vdots & \vdots \\ 0 & \dots & 0 & R & 0 \\ 0 & \dots & 0 & 0 & R \end{bmatrix}$$

with suitable dimensions. Substituting the system dynamic equation (16) into (18) yields

$$\bar{J}(x(\bar{k}),U(\bar{k})) = (\mathcal{A}x(\bar{k}) + \mathcal{B}U(\bar{k}))'\mathcal{Q}(\mathcal{A}x(\bar{k}) + \mathcal{B}U(\bar{k})) + U'(\bar{k})\mathcal{R}U(\bar{k}) \tag{19}$$

$$\bar{J}(x(\bar{k}),U(\bar{k})) = x'(\bar{k})\mathcal{A}'\mathcal{Q}\mathcal{A}x(\bar{k}) + 2x'(\bar{k})\mathcal{A}'\mathcal{Q}\mathcal{B}U(\bar{k}) + U'(\bar{k})(\mathcal{B}'\mathcal{Q}\mathcal{B} + \mathcal{R})U(\bar{k}) \tag{20}$$

With this open-loop approach it is easy to include constraints in the optimization problem as described in the following subsection.

6.3. MPC implementation

The value of the optimal control sequence $U^o(\bar{k})$ is computed using a suitable optimization routine that solves on-line the following Quadratic Programming (QP) problem:

$$U^o(\bar{k}) = \underset{U(\bar{k})}{\operatorname{argmin}} 0.5U(\bar{k})'HU(\bar{k}) + f'U(\bar{k}) \tag{21}$$

subject to

$A_v U(\bar{k}) = b_v$ linear equality constraints

$L_v U(\bar{k}) \le k_v$ linear inequality constraints

$l_v \le U(\bar{k}) \le u_v$ bound constraints

where

$H = 2\mathcal{B}'\mathcal{Q}\mathcal{B} + \mathcal{R}, \quad f = 2x(\bar{k})'\mathcal{A}'\mathcal{Q}\mathcal{B}$

$$L_v = \begin{bmatrix} -\mathcal{B} \\ \mathcal{B} \end{bmatrix}, \quad k_v = \begin{bmatrix} X_{bnd} + \mathcal{A}x(\bar{k}) \\ X_{bnd} - \mathcal{A}x(\bar{k}) \end{bmatrix}$$

$l_v = -u_{bnd}, \quad u_v = u_{bnd}$

where X_{bnd} is a column vector $\in \mathbb{R}^{4\cdot Nx1}$ defined as

$[x_{bnd}' \ x_{bnd}' \ x_{bnd}' \ x_{bnd}' \ \dots]'$

L_v and k_v are obtained expliciting the following constraints on the state prediction:

$$\begin{bmatrix} -X(\bar{k}) \\ X(\bar{k}) \end{bmatrix} \le \begin{bmatrix} X_{bnd} \\ X_{bnd} \end{bmatrix}$$

that using (16) results

$\mathcal{A}x(\bar{k}) + \mathcal{B}U(\bar{k}) \ge -X_{bnd}$

$\mathcal{A}x(\bar{k}) + \mathcal{B}U(\bar{k}) \le X_{bnd}$

that is

$-\mathcal{B}U(\bar{k}) \le X_{bnd} + \mathcal{A}x(\bar{k})$

$\mathcal{B}U(\bar{k}) \le X_{bnd} - \mathcal{A}x(\bar{k})$

which is exactly

$L_v U(\bar{k}) \le k_v$.

In runtime phase the following tasks are executed:

- connection with MATLAB;
- reading of the input analog channels of the I/O board to get the measures from the plant;
- state reconstruction through the Kalman filter;
- execution in the MATLAB environment, at each sampling instant, of the quadratic programming routine used to find the MPC control sequence;
- result retrievement from MATLAB workspace;
- writing of the output analog channel of the I/O board.

It is easy to figure out that this program structure is particularly suitable to explore the capabilities of the MPC algorithm, since all the computational part is delegated to MATLAB. The QP routine used is reliable, freeware, and fast and the C-MEX free source code is available. The software has been developed and compiled in Visual Studio 2005 and run on a Win32 architecture. The critical issue in the implementation of this code for a real-time application is represented by the execution time required by the Quadratic Programming routine that solves at each sampling time the optimization problem. Before proceeding with the

experiments it has been verified that with a sampling time of 0.03 s it is possible to respect the computational constraints within a prediction horizon N of 40 steps. For these experiments some modifications in the hardware are introduced: a faster PC mounting the I/O board RTI-DAC4 PCI by Inteco has been considered more suitable in this phase due to the increasing amount of the computational burden.

7. Experimental results

The results presented in this section intend to show the improvement that the MPC can introduce in a flexible arm motion regulation task, comparing its performance with a traditional LQR control scheme. To this aim four end-effector regulation experiments have been carried out, performing a 120° rotation maneuvers, using either the MPC or the LQR controller. The Kalman filter tuning never changes, in particular $diag\{\tilde{Q}\} = [100\ 100\ 100\ 100]$ and $diag\{\tilde{R}\} = [10^6\ 10^6]$.

Experiment 1. A 120° rotation maneuver is obtained using the LQR choosing $diag\{Q\} = [100\ 1\ 1\ 1]$, $R = 100$.

Experiment 2. A 120° rotation maneuver is obtained using a detuned version of the LQR with $diag\{Q\} = [100\ 1\ 1\ 1]$, $R = 1000$.

Experiment 3. A 120° rotation maneuver is obtained using the MPC with constraints on the input variable (motor torque), choosing $diag\{Q\} = [100\ 1\ 1\ 1]$, $R = 100$.

Experiment 4. A 120° rotation maneuver is obtained using the MPC with constraints on both input and state variable (see Table 3), choosing $diag\{Q\} = [100\ 1\ 1\ 1]$, $R = 100$.

The chosen controllers tuning is summarized in Table 3. $diag\{Q\} =$ is the vector whose elements constitute the diagonal of the state weights matrix Q, while R is the weight on the input. Q and R are the same for both the MPC and the LQR. T_s is the chosen sampling time. Comparing opportunely the resulting responses, remarkable observations follow.

Comparison 1: Experiment 1 vs Experiment 3. The MPC with constraints on the input variable introduces a marginal performance improvement if compared with the LQR response as shown in Figs. 15 and 18. This is due to the capability of the MPC to constrain the motor torque (Fig. 16).

Comparison 2: Experiment 1 vs Experiment 4. MPC gets to keep oscillations within the specified bounds during the maneuver. The oscillations reduction is larger than the desired level due to model deflections overestimation. For this reason the constraint threshold loses a precise numerical meaning but it can be considered as a knob to regulate the maximum amplitude of the oscillations (Fig. 18).

Table 2
Model parameters.

Parameter	Value
ξ	0.034
I	$2.95E^{-11}$ m^4
J_p	$1.73E^{-5}$ kg m^2
τ_s	0.065 Nm
τ_c	0.0055 Nm
τ_{max}	0.214 Nm
E	6.4081 GPa
J_0	0.0016 kg m^2
L	0.387 m
ρ	0.09 kg/m
m_p	0.155 kg
τ_{min}	−0.214 Nm

Table 3
MPC and LQR parameters.

Parameter	Value
N	40
S	$\overline{P}$
$diag\{Q\} =$	[100 1 1 1]
R	100
$diag\{\tilde{Q}\} =$	[100 100 100 100]
$diag\{\tilde{R}\} =$	$[10^6\ 10^6]$
Detuned LQR R	[1000]
u_{bnd}	0.214
x_{bnd}	$[\infty\ \infty\ 0.0027\ \infty]^T$
T_s	0.03

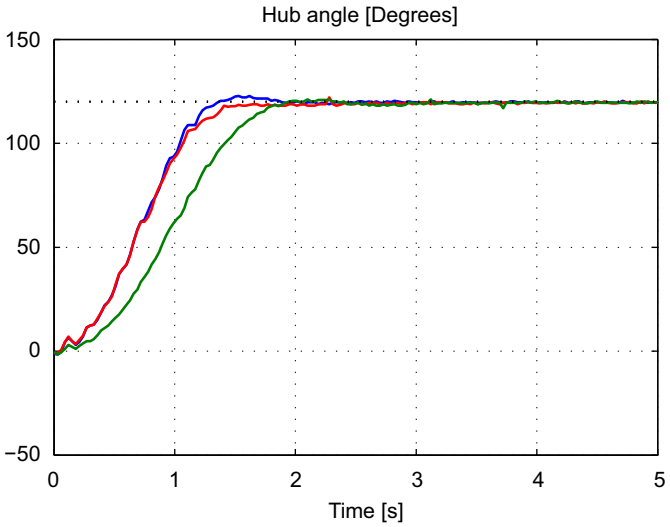

Fig. 15. Experimental comparison. Blue line: Experiment 1 (LQR). Red line: Experiment 3 (input constrained). Green line: Experiment 4 (full constrained MPC). (For interpretation of the references to color in this figure legend, the reader is referred to the web version of this article.)

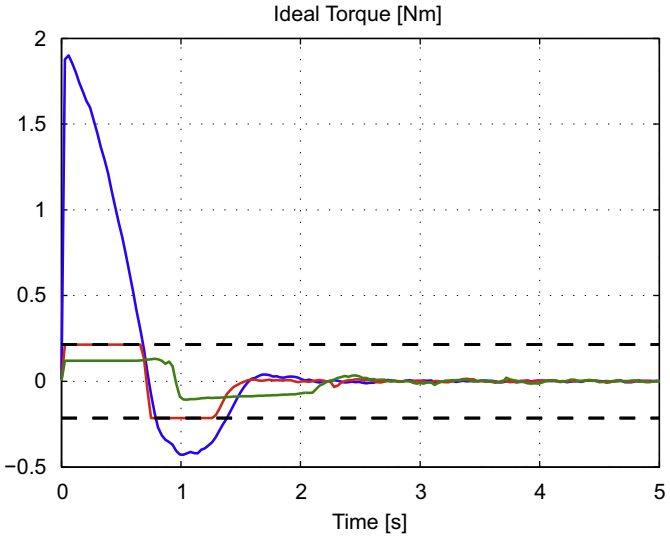

Fig. 16. Experimental comparison. Blue line: Experiment 1 (LQR). Red line: Experiment 3 (input constrained). Green line: Experiment 4 (full constrained MPC). (For interpretation of the references to color in this figure legend, the reader is referred to the web version of this article.)

In Fig. 15 it is easy to see that a time delay in the motor hub positioning is introduced when constraints on maximum deflection are present. In fact in order to reach this aim the actuator

effort needs to be reduced (see Fig. 17). Nevertheless it is interesting to observe in the same figure that the actuator command profile generated through the MPC is close to a bang profile that satisfies time optimality criteria.

Comparison 3: Experiment 1 vs Experiment 2 vs Experiment 4. Fig. 22 shows that the deflection amplitude of the detuned version of the LQR is reduced but it cannot reach the required reduction level. In fact in the first part of the response the deflection is out of the specified bound. Higher value of R should be chosen in order to reach the desired aim. Nevertheless this result cannot be achieved as Figs. 19–21 points out. In fact the reduction of the actuator effort resulting from the choice of increasing value of R leads to non-negligible positioning errors (Fig. 19). This result underlines the importance of the capability of the MPC to handle constraints.

8. Conclusions

In this work the Model Predictive Control is applied for the first time to control the motion of a flexible arm. The non-linear model, identified and validated with experimental data, is a critical achievement, exploited for the tuning of the MPC controller. The obtained results give experimental evidence of the capability of MPC to maximize the utilization of the actuator effort, maintaining under control the arm oscillations also during the maneuver. These features differentiate MPC from any other controller synthesized on linear models, for which the only possibility to satisfy input and output constraints is to detune the controller, with consequent performance degradation. The experimental results are a significant contribution of this work and have been obtained through the development of a suitable software solution that allows to interface the optimization

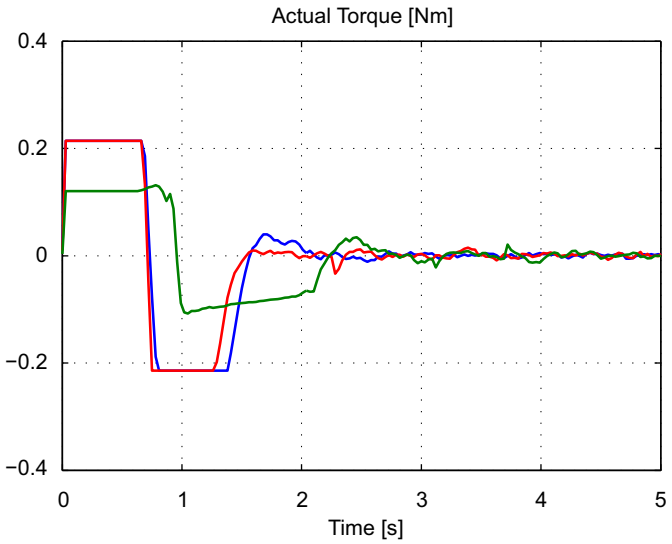

Fig. 17. Experimental comparison. Blue line: Experiment 1 (LQR). Red line: Experiment 3 (input constrained). Green line: Experiment 4 (full constrained MPC). (For interpretation of the references to color in this figure legend, the reader is referred to the web version of this article.)

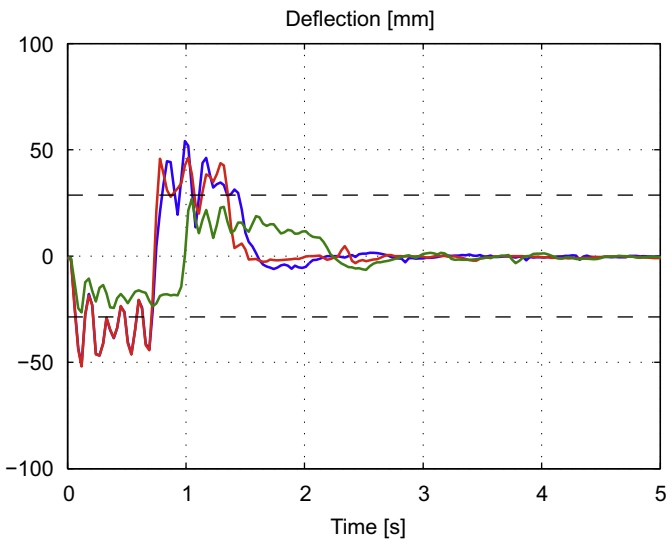

Fig. 18. Experimental comparison. Blue line: Experiment 1 (LQR). Red line: Experiment 3 (input constrained). Green line: Experiment 4 (full constrained MPC). (For interpretation of the references to color in this figure legend, the reader is referred to the web version of this article.)

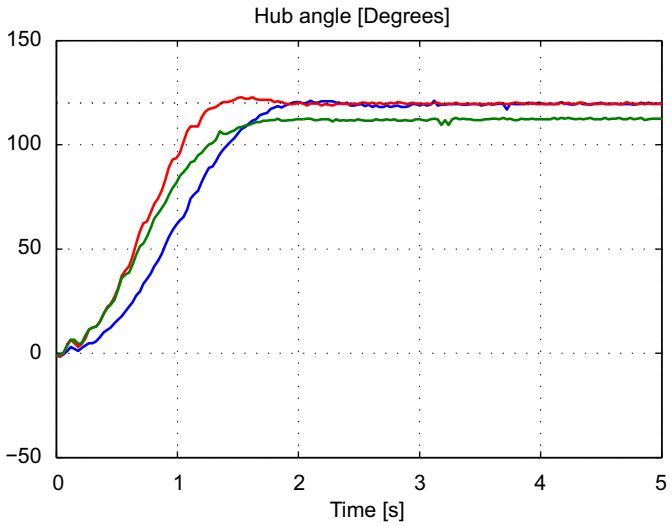

Fig. 19. LQR detuning. Red line: Experiment 1 (LQR, $R=100$). Blue line: Experiment 4 (MPC $R=100$). Green line: Experiment 2 (Detuned LQR, $R=1000$). (For interpretation of the references to color in this figure legend, the reader is referred to the web version of this article.)

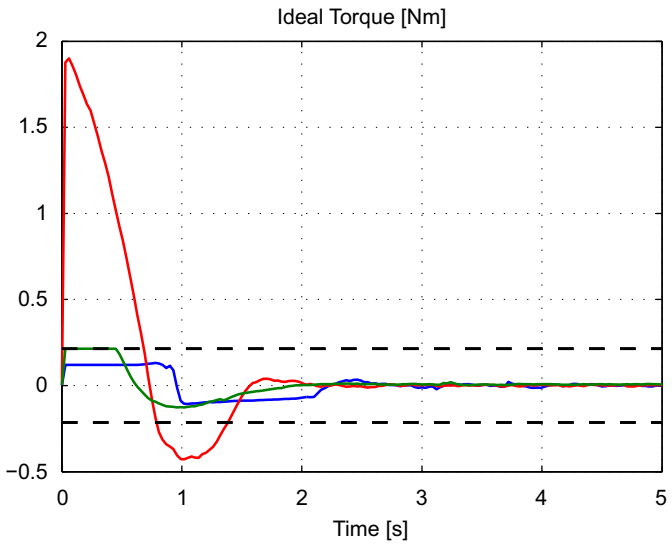

Fig. 20. LQR detuning. Red line: Experiment 1 (LQR, $R=100$). Blue line: Experiment 4 (MPC $R=100$). Green line: Experiment 2 (Detuned LQR, $R=1000$). (For interpretation of the references to color in this figure legend, the reader is referred to the web version of this article.)

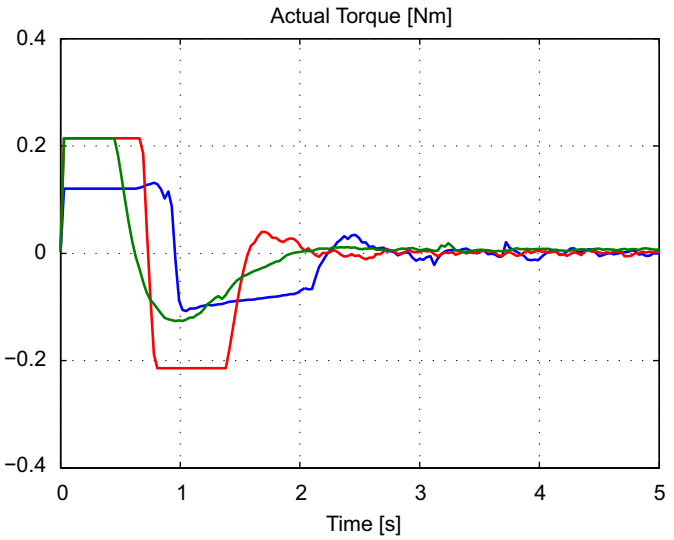

Fig. 21. LQR detuning. Red line: Experiment 1 (LQR, $R=100$). Blue line: Experiment 4 (MPC $R=100$). Green line: Experiment 2 (Detuned LQR, $R=1000$). (For interpretation of the references to color in this figure legend, the reader is referred to the web version of this article.)

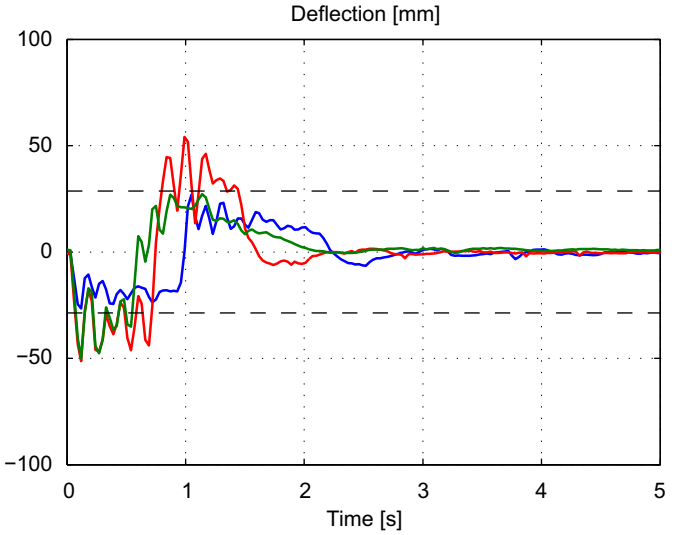

Fig. 22. LQR detuning. Red line: Experiment 1 (LQR, $R=100$). Blue line: Experiment 4 (MPC $R=100$). Green line: Experiment 2 (Detuned LQR, $R=1000$). (For interpretation of the references to color in this figure legend, the reader is referred to the web version of this article.)

algorithm with the sensors and the actuator. In the future, more work could be done in order to understand the possible improvement achievable with a reduction of the sampling time. Moreover, based on the observation that one of the most effective strategy used in the field of vibration suppression is represented by reference pre-shaping, MPC controller can be thought as an automatic tool to give, in closed loop, a shaped position reference for an existing position control loop. This hierarchical scheme provides good performance in many applications where MPC is used to generate the set-point for another faster regulator (Scattolini, 2009). Final results could be extended to trajectory control of multilink robotic arms.

References

Balas, M. (1978). Feedback control of flexible systems. *IEEE Transactions on Automatic Control*, *23*(4), 673–679.

Bascetta, L., & Rocco, P. (2006). Two-time scale visual servoing of eye-in-hand flexible manipulators. *IEEE Transactions on Robotics*, *22*, 818–830.

Bayo, E., Papadopoulos, P., Stubbe, J., & Serna, M. A. (1989). Inverse dynamics and kinematics of multi-link elastic robots: An iterative frequency domain approach. *The International Journal of Robotics Research*, *8*(6), 49–62.

Benosman, M., & Le Vey, G. (2004). Control of flexible manipulators: A survey. *Robotica*, *22*, 533–545.

Bernelli-Zazzera, F., Romano, M., Casciati, F., Faravelli, L., Frosini, L., & Gallone, S. (2001). Multiobjective onboard experiment for advanced researches on robotics, control systems and materials behaviour. *Microgravity and Space Station Utilization*, *2*, 15–17.

Book, W. J. (1993). Structural flexibility of motion systems in the space environment. *IEEE Transactions on Robotics and Automation*, *9*, 524–530.

Boscariol, P., Gasparetto, A., & Zanotto, V. (2010). Model predictive control of a flexible links mechanism. *Journal of Intelligent and Robotic Systems*, *58*(2), 125–147.

Boscariol, P., Gasparetto, A., & Zanotto, V. (2009). Vibration reduction in a flexible link mechanism through the synthesis of an MPC controller, In *Proceedings of international conference on mechatronics* (pp. 1–6), Malaga, Spain.

Cannon, J., & Schmitz, E. (1984). Initial experiments on the end-point control of a flexible one-link robot. *The International Journal of Robotics Research*, *3*(3), 62–75.

Canudas de Wit, C., Bastin, G., & Siciliano, B. (1996). *Theory of robot control*. New York: Springer-Verlag.

Dwivedy, S. K., & Eberhard, P. (2006). Dynamic analysis of flexible manipulators, a literature review. *Mechanism and Machine Theory*, *41*, 749–777.

Gurtin, M. E. (1981). *An introduction to continuum mechanics*. New York: Academic Press.

Hassan, M., Dubay, R., Li, C., & Wang, R. (2007). Active vibration control of a flexible one-link manipulator using a multivariable predictive controller. *Mechatronics*, *17*(6), 311–323.

Lovekin, D., Hepplerand, J., & McPhee, J. (2000). Design and analysis of a facility for free-floating flexible manipulators. *Transactions of the CSME*, *24*(2), 375–390.

Martins, J. M., Mohamed, Z., Tokhi, M. O., Sa da Costa, J. S., & Botto, M. A. (2003). Approaches for dynamic modelling of flexible manipulator systems. *Control Theory and Applications. IEEE Proceedings*, *150*(4), 401–411.

Meirovitch, L. (1967). *Analytical methods in vibrations*. MacMillan Publishing.

Mimmi, G., Rottenbacher, C., & Bonandrini, G. (2008). Theoretical and experimental sensitivity analysis of extra insensitive input shapers applied to open loop control of flexible arm. *International Journal of Mechanics and Materials in Design*, *5*(1), 61–67.

Mohamed, Z., Martins, J., Tokhic, M., Sá da Costa, J. S., & Botto, M. A. (2005). Vibration control of a very flexible manipulator system. *Control Engineering Practice*, *13*, 267–277.

Mohamed, Z., & Tokhi, M. O. (2003). Hybrid control schemes for input tracking and vibration suppression of a flexible manipulator. *Proceedings of the Institution of Mechanical Engineers, Part I: Journal of Systems and Control Engineering*, *217*, 23–34.

Olsson, H., Aström, K., Canudas-de Wit, C., Gäfvert, M., & Lischinsky, P. (1998). Friction models and friction compensation. *European Journal of Control*, *4*, 176–195.

Pereira, E., Diaz, I. M., Cela, J. J. L., & Feliu, V. (2007). A new design methodology for passivity-based control of single-link flexible manipulators. In *Advanced intelligent mechatronics* (pp. 1–6).

Rao, S. S. (2003). *Mechanical vibrations* (4th ed.). Prentice-Hall.

Scattolini, R. (2009). Architectures for distributed and hierarchical model predictive control a review. *Journal of Process Control*, *19*, 723–731.

Siciliano, B., & Book, W. J. (1988). A singular perturbation approach to control of lightweight flexible manipulators. *The International Journal of Robotics Research*, *7*(4), 79–90.

Uchiyama, M., Konno, A., Uchiyama, T., & Kanda, S. (1990). Development of a flexible dual-arm manipulator testbed for space robotics, In: *IEEE international workshop on intelligent robots and systems '90. Towards a new frontier of applications, proceedings. IROS'90.*

Wang, D., & Vidyasagar, M. (1991). Control of a class of manipulators with a single flexible link: Part i. Feedback linearization. *Journal of Dynamic Systems, Measurement, and Control*, *113*(4), 655–657.

Wang, Y., & Boyd, S. (2008). Fast model predictive control using online optimization, In *Proceedings IFAC world congress* (pp. 6974–6997), Seoul, Italy.

Yuan, B., Book, W. J., & Siciliano, B. (1989). Direct adaptive control of a one-link flexible arm with tracking. *Journal of Robotic Systems*, *6*(6), 663–680.